

Elucidation of the myrcene ozonolysis mechanism from a Criegee Chemistry perspective

Meifang Chen^{1,2}, Shengrui Tong^{1,*}, Shanshan Yu¹, Xiaofan Lv^{1,2}, Yanyong Xu^{1,2}, Hailiang Zhang¹, Maofa Ge^{1,2}

5 ¹State Key Laboratory for Structural Chemistry of Unstable and Stable Species, Beijing National Laboratory for Molecular Sciences (BNLMS), Institute of Chemistry Chinese Academy of Sciences, Beijing 100190, P.R. China.

²University of Chinese Academy of Sciences, Beijing 100049, P.R. China.

Correspondence to: Shengrui Tong (tongsr@iccas.ac.cn)

Abstract. Criegee intermediates (CIs) are highly reactive species generated during the alkene ozonolysis, which play a critical
10 role in atmospheric chemistry. Myrcene is a typical monoterpene, and its linear structure is significantly different from other
cyclic monoterpenes such as α -pinene. This structural distinction consequently leads to different reactions mechanisms. This
study employs a combined approach of matrix isolation Fourier transform infrared spectroscopy (MI-FTIR) and smog chamber
experiments to elucidate the mechanisms of myrcene ozonolysis from the Criegee chemistry perspective. C3-CIs are captured
at 880 cm⁻¹ by using MI-FTIR. Ordered oligomers, which contain C3-CIs as chain units, are detected as significant components
15 in secondary organic aerosol (SOA). These oligomers are formed via RO₂ + n C3-CIs + HO₂/RO₂ mechanisms. Two CIs with
different molecular sizes, C3-CIs and C7-CIs, are captured at 880 and 905 cm⁻¹ by using MI-FTIR. Ordered oligomers with
C3-CIs serving as chain units, formed via RO₂ + n C3-CIs + HO₂ and RO₂ + n C3-CIs + RO₂ mechanisms, are detected as
significant components in secondary organic aerosol (SOA). C7-CIs are more prone to unimolecular
decomposition/ degradation to form C7-RO₂ radical, which act as initiators for oligomerization reactions. The mechanisms may
20 also exist in other monoterpenes ozonolysis, which offering new insights into the contribution of CIs to SOA formation.
Furthermore, the effect mechanisms of the synergistic interaction between SCIs oligomerization and RO₂ autoxidation are
illustrated. The mechanisms facilitate the rapid formation of highly oxygenated species, playing a critical role in particle
nucleation. The increase in relative humidity can effectively reduce the formation of higher-order oligomers, thereby
suppressing the SOA yields. This study provides a systematic elucidation of myrcene ozonolysis mechanisms, thereby
25 significantly enhancing the understanding of oxidation processes in acyclic monoterpenes.

1. Introduction

Criegee Chemistry has long been recognized as playing an important role in tropospheric atmosphere. Multiple model
simulations have yielded atmospheric concentrations of stabilized Criegee intermediates (SCIs) of around 10⁴–10⁵ molecules
cm⁻³ (Khan et al., 2018; Chhantyal-Pun et al., 2020). The concentration of OH radical is about 10⁶ molecules cm⁻³ (Ringsdorf
30 et al., 2023; Hofzumahaus et al., 2009; Lelieveld et al., 2016). Typically, if k_{SCI} is ~100 times larger than k_{OH}, this is enough

to make the rate of loss for reaction with SCIs comparable to that for reaction with OH radical. SCIs can undergo **extremely** rapid reactions with many common trace molecules in the atmosphere, such as SO₂, organic acids, and amides, which are also faster than that reactions with OH radical (Long et al., 2025; Welz. O. et al., 2014; Chhantyal-Pun et al., 2015; Mauldin et al., 2012). Recent study has shown that SCIs are significantly more efficient at removing greenhouse gases ((CF₃)₂CFCN) than OH radical (Jiang et al., 2025). The reaction with water vapor is the main removal pathway for SCIs due to the **extremely** high abundance of water vapor in the atmosphere. The reaction rates of SCIs of different configuration with water vapor are found to be 10⁻¹¹-10⁻²⁰ cm³ molecule⁻¹ s⁻¹. Among them, the reaction rate of syn-CH₃CHOO with H₂O is approximately 10⁻¹⁹-10⁻²⁰ cm³ molecule⁻¹ s⁻¹, while the reaction rate of anti-CH₃CHOO with H₂O is faster, at approximately 10⁻¹⁴ cm³ molecule⁻¹ s⁻¹ (Vereecken et al., 2022; Yin and Takahashi, 2018; Lin et al., 2016; Anglada and Sole, 2016; Taatjes et al., 2013). The reaction has a pronounced conformational dependence, leading to large differences in reaction rates. Similarly, the reactivity of SCIs unimolecular **decompositiondegradation** is also conformation-dependent. Compared to anti-CIs, syn-CIs are more prone to undergo unimolecular **decompositiondegradation** reactions (Long et al., 2018, 2019; Vereecken et al., 2017).

The unimolecular **degradationdecomposition** process of SCIs, as well as bimolecular reactions involving organic acids, RO₂, etc. contribute significantly to the formation and growth of atmospheric secondary organic aerosol (SOA) (Boy et al., 2013; Chen et al., 2022; Zhao et al., 2015). Both field observations and laboratory studies have revealed that smaller-sized SCIs undergo sequential oligomerization reactions with RO₂ and organic acids, leading to the formation of low volatility organic compounds (LVOCs) or extremely low volatility organic compounds (ELVOCs) (Luo et al., 2025). Oligomers with CH₃CH₂CHOO (SCIs) as chain units were observed during the trans-3-hexene ozonolysis process (Zhao et al., 2015). Early studies on ethylene ozonolysis also identified oligomers formed from the reaction of multiple CH₂OO with organic acids (Sakamoto et al., 2013; Chen et al., 2021). Caravan et al. observed the oligomer sequence obtained through the continuous reaction of formic acid and six CH₂OO in the Central Amazon region (Caravan et al., 2024). These direct evidences indicate that SCIs contribute to SOA formation by oligomerization. These oligomerization mechanisms are now widely observed in the ozonolysis of alkenes that generate small-sized SCIs. Relative humidity (RH) may affect ozonolysis systems through the direct reactions between water vapor and SCIs. Zhang et al. found that **SOA yield form limonene ozonolysislimonene yield** gradually increased with increasing RH, while SOA yield from Δ³-carene ozonolysis decreased slightly. They attributed this phenomenon to the differing volatility of the products resulting from the reaction of structurally distinct CIs generated from the ozonolysis of these two monoterpenes with H₂O (Zhang et al., 2023). Quantum chemical calculations have revealed that multiple SCIs may undergo oligomerization reactions with **hydroperoxide esters (the products of the reaction of CH₂OO with water)water vapor** to form oligomers with lower volatility (Chen et al., 2019). Increasing RH has been found to result in lower SOA yields and reduced oligomerization during the cis-3-hexenol ozonolysis (Harvey et al., 2016). The addition of water alters the reaction mechanism of SCIs in the ozonolysis system, leading

to changes in the particle composition, which in turn affects the SOA yield. This indicates that RH is a key factor influencing the ozonolysis mechanism.

65 Monoterpenes ($C_{10}H_{16}$) emit into the atmosphere at a mean global rate of 95×10^6 metric tons of carbon per year, and contribute significantly to the global SOA budget. The yields of SCIs obtained from monoterpene ozonolysis ranges from approximately 0.2 to 0.60 (Sipila et al., 2014; Zhang and Zhang, 2005; Gong and Chen, 2021; Cox et al., 2020; Newland et al., 2018). The high yield leads to the occurrence of numerous SCIs-related reactions. Products derived from SCIs are also significant components of the SOA generated from monoterpene ozonolysis. Both in the α -pinene and
70 limonene ozonolysis, specific mechanisms have been proposed in which both the unimolecular channels and the bimolecular reactions of SCIs contribute to the formation of SOA~~SCIs-derived products contribute to both monomers and dimers formation of SOA~~ (Zhao et al., 2021; Zhang et al., 2023). The emissions of myrcene account for 2% to 10% of total biogenic monoterpene emissions (Sindelarova et al., 2014; Helmig et al., 2013). In addition to biogenic emissions, myrcene can also be present in indoor air (Kostiainen, 1995). The reaction with O_3 is one of the main removal pathways
75 in myrcene, and plays an important role in the particle formation in the atmosphere. Myrcene is a straight-chain alkene containing both a conjugated π system, similar to that of isoprene ($CH_2=CH-C(=CH_2)$ -moiety), and a second part, structurally analogous to 2-methyl-2-butene ($(CH_3)_2C=CH$ -moiety, which is different from most of the widely studied cyclic monoterpenes (e.g., α -pinene, limonene). Such structural differences may give rise to variations in the reaction mechanisms and kinetics. The reaction rate of myrcene with O_3 is $3.8 \times 10^{-16} \text{ cm}^3 \text{ molecule}^{-1} \text{ s}^{-1}$, approximately 50 times
80 faster than that of α -pinene ozonolysis and nearly 2 times faster than that of limonene ozonolysis (Deng et al., 2018; Atkinson et al., 1990; Cox et al., 2020; Munshi et al., 1989). About 99% of the O_3 addition reactions with myrcene occur at the isolated double bond ($(CH_3)_2C=CH-CH_2-$ moiety) (Deng et al., 2018). Therefore, the myrcene ozonolysis can lead to the formation of two CIs, $C_7H_{10}O_2$ (C7-CIs) and $C_3H_6O_2$ (C3-CIs). For cyclic monoterpenes such as α -pinene and limonene, their ozonolysis processes can only produce larger CIs containing ten carbon atoms (C10-CIs). Current
85 studies have not confirmed that the C10-CIs generated from monoterpene ozonolysis can contribute to SOA formation through oligomerization. This suggests that the contribution mechanisms of CIs of different sizes produced during monoterpene ozonolysis to SOA formation may differ. Further studies are needed to elucidate the distinct roles of these CIs with different molecular sizes in SOA formation mechanisms, as well as the influence of their interactions on particle formation.

90 In this work, matrix isolation technology combined with vacuum Fourier transform infrared spectroscopy (MI-FTIR) and a smog chamber were employed to investigate the roles of both C3-CIs and C7-CIs in the myrcene ozonolysis. MI-FTIR was used to characterize the key intermediates produced in the early stage of myrcene ozonolysis, which to confirm the formation of stable C3-CIs and C7-CIs. To get the contribution mechanism of C3-CIs and C7-CIs to SOA, we also performed the smog chamber experiments in various conditions during myrcene ozonolysis. RH was also considered as

95 a significant factor influencing the ozonolysis mechanism and taken as an experimental variable. By analyzing the yields and molecular compositions of SOA, we elucidated distinct formation mechanisms through which varying molecular sizes of CIs contribute to SOA formation. Integrating these advanced techniques effectively improved the understanding of myrcene-derived SOA formation mechanism from the Criegee chemistry perspective.

2. Materials and methods

100 2.1 Matrix isolation experiment

Myrcene (97%, Aladdin) was further purified through three freeze-pump-thaw cycles before being stored as a liquid in a storage tube. The O₂/O₃ mixture was produced by a high-voltage discharge type ozone generator (Beijing Tonglin Technology Co., LTD). The collected O₂/O₃ mixture was frozen in liquid nitrogen and undergoes several cycles of freezing pump - thawing to remove the residual impurity gas. O₃ or myrcene, in a 1:100 ratio with Ar, was mixed and stored in a 5 L spherical glass container. The matrix was maintained at 6±1 K within a closed-cycle helium refrigerator (Physike Technology Co., LTD, Qcryo-Scryo-S-300). The characteristic infrared peaks of initial ozonolysis products were detected by using a Fourier transform infrared spectrometer (Bruker Vertex 70v) equipped with a liquid nitrogen-cooled mercury-cadmium-telluride (MCT) detector. Measurements spanned 600-4000 cm⁻¹, employing 32-scan averaging and 0.5 cm⁻¹ resolution. The experimental chamber was maintained under a vacuum of 10⁻⁵ Pa. The deposition of myrcene/Ar and O₃/Ar onto the 6±1 K cold window was facilitated by two angled and independent tubes at a rate of 5 ml/min., thereby ensuring a brief mixing period for the reactants before deposition. This deposition was known as the twin-jet co-deposition mode. The deposition duration was approximately 120 min. To allow limit the diffusion and/or reaction of reactants, these matrices were heated or annealed to 35 K and held for 0.5 h, and then cooled to 6±1 K after which the spectra were recorded. To promote the further occurrence of the reaction and further soften and diffuse the matrix, the matrix was further heated to 45 and 55 K (Yu et al., 2025; Yang et al., 2020). To prevent matrix loss, it was imperative to immediately cool down to 6±1 K after reaching the target temperature and to record the spectra.

2.2 Particles generation and collection

The myrcene ozonolysis experiments were performed in a 1.2 m³ atmospheric simulation Teflon chamber maintained at room temperature (24±1 °C) under different RH conditions. Myrcene was introduced into the chamber by passing zero air through a heated three-way U-shaped tube. The addition of formic acid and n-hexane was conducted in a consistent manner. The addition of approximately 367 ppm of n-hexane resulted in the removal of approximately 989% of OH radical. An O₂/O₃ mixture was generated by passing high-purity O₂ (≥99.999%) at a flow rate of 200 mL/min through an ozone generator (Beijing Tonglin Technology Co., Ltd.). Formic acid was added about 0.65 ppm. Subsequently, the O₂/O₃ mixture was injected into the

chamber through a syringe. The O₂/O₃ mixture was introduced in a single injection via a syringe and was not replenished during the experiment. The O₃ concentration was monitored by an O₃ analyzer (Thermo Scientific model 49i) throughout myrcene ozonolysis. The measurement of the myrcene concentration was conducted by means of a gas chromatograph with a quadrupole mass spectrometer (GC-MS, Agilent, 7890, 5977B) equipped thermal desorption instrument (TD). The GC-MS is on an 2P-5MS column (30 m × 0.25 × 5 mm) with helium as carrier gas and a flow rate of 1.2 mL/min. The temperature of the chromatographic column was set as follows: the initial temperature was 40 °C and held for 3 minutes. The temperature was then increased to 140 °C by maintaining a rate of 20 °C/min; the program was then finished by increasing the temperature to 200 °C at a rate of 25 °C/min. Organics were quantified with mode selection SIM and 41 m/z, 69 m/z and 93 m/z were selected as the characteristic ions detected by mass spectrometry for myrcene. The maintenance of different RH levels was achieved by the implementation of a 10 L/min flow of zero air through the water bubbler. The indoor temperature and RH were measured using a hygrometer (Vaisala, HMP3). Throughout each experiment, size distributions and volume concentrations of particles were continuously recorded using a scanning mobility particle sizer (SMPS), which consisted a differential mobility analyzer (DMA, TSI, Model 3081) and a condensation particle counter (CPC, TSI, Model 3776). The SMPS measured particles every 3 minutes across a size range of 14.3 to 723.4 nm. A sampling flow of 0.3 L min⁻¹ and a sheath flow of 3.0 L min⁻¹ were used. The yield of SOA was obtained by the ratio of the maximum mass concentration of the corrected particles to the mass concentration of myrcene consumed (Liu et al., 2024; Chen et al., 2022). The specific equation was as follows.

$$Y_{\text{SOA}} = \frac{M_{\text{SOA}}}{\Delta M_{\text{VOC}}}$$

Here, Y_{SOA} represented the SOA yield, M_{SOA} denoted the maximum mass concentration of particle after wall-loss correction during the reaction process, and ΔM_{VOC} referred to the total consumption mass concentration of VOCs throughout the reaction.

The average effective density of SOA obtained from the myrcene ozonolysis is 1.25 g cm⁻³ (Boge et al., 2013). The SOA was sampled after 3 hours of reaction, with a sampling duration of approximately 60 minutes. The SOA particles generated within

the chamber were captured on a 25 mm PTFE filter (Sartorius, 0.45 μm pore size) and subsequently analyzed using an ultra-high performance liquid chromatography with a Quadrupole-Orbitrap mass spectrometer equipped with an electrospray ionization source (UHPLC/ESI-MS, UPLC, UltiMate 3000, Thermo Scientific, ESI-MS, Q-Exactive, Thermo Scientific) equipped with a Hypersil GOLD C18 column (2.1 × 100 mm, 1.9 μm packing size Thermo Scientific). The collected particle sample was eluted with 0.5 ml of methanol (Optima™ LC/MS Grade, Fisher Chemical) into a sample bottle. Mass spectrometric analysis utilized positive ion mode, scanning a molecular weight range of m/z 50–750 Da. The elution flow rate was set at 0.2 mL/min with a total run time of 4.0 min. An injection volume of 10 μL was used. In positive ion mode, three ionic forms of particulate components were identified, specifically [M+H]⁺, [M+Na]⁺ and [M+NH₄]⁺. Tandem mass spectrometry (MS/MS) was employed to elucidate component structures within the SOA. The isolation width of 1.2 m/z units was applied. The electrospray ionization source was operated at a spray voltage of 3.0 kV and a capillary temperature of 300 °C.

155 with sheath and auxiliary gas flows set to 35 and 10 Arb units, respectively. Both scans were performed at a resolution setting defined at m/z 200, with values of $R = 70,000$ for the MS scan and $R = 17,500$ for the MS/MS scan. Data acquisition and processing were conducted using Xcalibur software (version 3.0).

2.3 Quantum chemistry calculations

160 Additional quantum chemical calculations were performed to compare with the experimentally obtained infrared spectra. The geometries of the myrcene, primary ozonides (POZs) and SCIs were optimized using the hybrid density functional theory B3LYP-D3(BJ) with the aug-cc-pVTZ basis set. Harmonic vibrational frequencies were calculated at B3LYP/6-311G++(d,2p) calculation level for the comparison with the experimental infrared peak. Various computational levels for CIs were compared, and the one with superior performance was selected accordingly. Please refer to Table S1 for the specific comparison. ~~Harmonic and anharmonic vibrational frequencies were calculated at the same calculation level for the comparison with the experimental~~

165 ~~infrared peak.~~ This method has been proved to be applicable to the relevant calculations of the SCIs system (Chen et al., 2025; Lin et al., 2018; Yu et al., 2025). The above-mentioned related calculations were all performed by using Gaussian 16 software package (Frisch et al., 2016). Molclus 1.1.2 in conjunction with the xtb software package was used to perform a systematic conformational search for myrcene, POZs and SCIs (Lu, 2023). The single-point energy was further calculated at the DLPNO-CCSD(T)/CBS level by using ORCA 5.0 software to obtain the Boltzmann distribution of each conformation more accurately

170 (Neese, 2022).

3. Results and Discussion

3.1 Criegee chemistry in myrcene ozonolysis

$C_7H_{10}O_2$ (C7-CIs) and $C_3H_6O_2$ (C3-CIs) was produced from myrcene ozonolysis. The initial ozonolysis mechanism of myrcene had been established as shown in Figure 1 based on the current studies. The products generated along with C7-CIs and C3-CIs were acetone and 4-vinyl-4-pentenal (C7-aldehyde) with yields of 0.27 and 0.73, respectively (Deng et al., 2018). The nascent C7-CIs and C3-CIs, possessing high internal energy, rapidly degraded in part. This process could contribute to the formation of OH radical (R2 and R3). This process could contribute to the formation of OH radical. The unimolecular isomerization pathways of CIs were strongly configuration-dependent. Syn-C7-CIs were mainly isomerized by 1,4-H transfer to form vinyl hydroperoxide (VHP), which decomposed to form OH radical and a vinoxy or β -oxo alkyl radical (R2 and R4). Anti-C7-CIs

175

180 mainly proceed an initial rearrangement (1,3 ring-closure) to form a dioxirane intermediate. Then the dioxirane intermediates could isomerize to form organic acid (R3 and R5). $C_3H_6O_2$ isomerized mainly through the formation of VHP. Another portion was collisional stabilized, forming SCIs (R1) (Criegee, 1975; Hassan et al., 2021; Jr-Min Lin and Chao, 2017; Khan et al., 2018). A portion of the SCIs might undergo unimolecular decomposition~~degradation~~ reactions, while another portion primarily

engaged in bimolecular reactions with trace gases in the atmosphere (Jr-Min Lin and Chao, 2017; Kidwell et al., 2016; Su et al., 2014; Vereecken et al., 2012). The yields of OH radical and SCIs obtained from the myrcene ozonolysis were 0.63 ± 0.09 and 0.30, respectively (Cox et al., 2020; Newland et al., 2018).

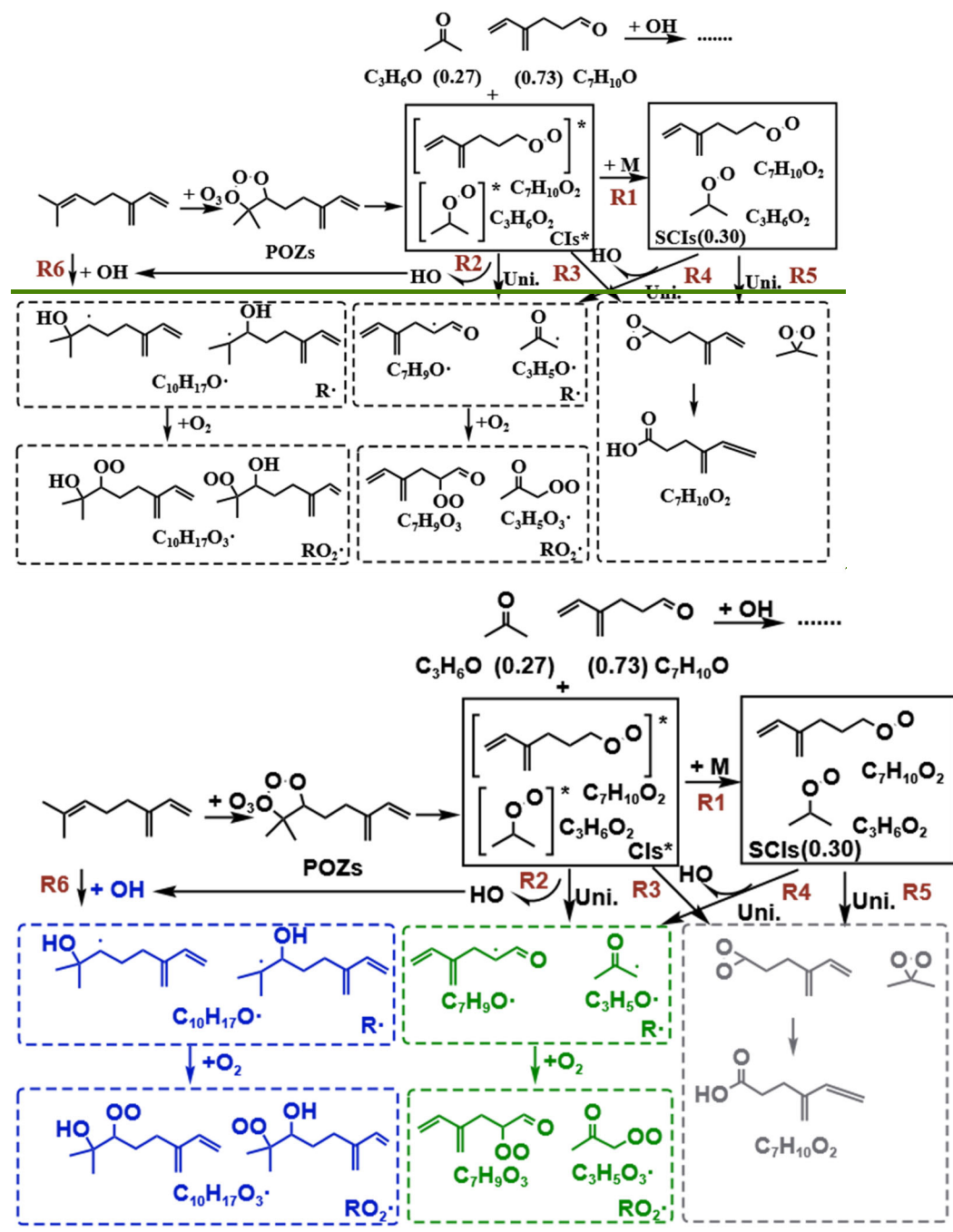


Figure 1 Proposed the key pathway in the initial ozonolysis of myrcene. The values in parentheses represent the yields of the corresponding products. The blue boxes indicate OH-derived products. Green-shaded boxes represent products formed via unimolecular reaction of syn-CIs through the vinylhydroperoxide (VHP) channel followed by O₂ addition. Gray-shaded boxes correspond to products generated from unimolecular reaction of anti-CIs via 1,3-ring-closure.

Although previous studies had provided some references to the initial ozonolysis mechanism of myrcene, the presence of CIs had only been demonstrated deductively. In this study, MI-FTIR was employed to capture the key intermediates formed during the initial ozonolysis of myrcene. As shown in Figure 2, some new bands were observed in the spectra obtained by the twin-jet co-deposition. Most of the absorption peaks of the products grew with rising temperature within the 35-55 K interval. This

observation indicated that the myrcene initial ozonolysis occurred when the Ar matrix softened and diffused. The new bands were located at 765, 880, 905, 1074, 1177, 1370 and 1720 cm^{-1} . The spectra of a single precursor (Myrcene/Ar or O_3/Ar) obtained after annealing at different temperatures as comparison was shown in Figure S1.

200 The characteristic IR vibrational bands of the POZs, formed via initial cycloaddition between myrcene and O_3 , were localized on its 1,2,3-trioxolane ring. These included asymmetric O-O-O stretching and C-O stretching vibrations within the five-membered ring structure (Wang et al., 2020). The presence of two different configurations in POZs was attributable to the varying orientations of the central O atom on the five-membered ring. The peaks calculated from the asymmetric stretching vibration in both POZs configurations overlapped at 772 cm^{-1} . Moreover, O-O-O asymmetric stretching vibrations of POZs
205 were commonly observed within the 700-800 cm^{-1} spectral region as documented in prior literature (Yang et al., 2020; Wang, 2020). Thus, the band at 765 cm^{-1} which obtained from the twin-jet experiment was assigned to the O-O-O asymmetric stretching vibration of POZs. The calculation results indicated that the C-O stretching vibrations of the two POZs were located at positions 105968 and 116574 cm^{-1} . The newly emerged peaks at positions 1074 and 1177 cm^{-1} corresponded to the C-O stretching vibration of POZs in the twin-jet spectra. Moreover, these POZ-related infrared peaks emerged at 35 K, and their
210 intensity increased with rising annealing temperature until distinct infrared peaks became apparent at 55 K.

The main conformers and the infrared vibration frequencies of C3- and C7-CIs were obtained through quantum chemical calculations. The strongest characteristic infrared vibration peak of CIs was caused by O-O stretching vibration (Su et al., 2013; Lin et al., 2015). The extant research results indicated that the characteristic infrared peak caused by the O-O stretching vibration of C3-CIs in the gas phase located at 887 cm^{-1} (Wang et al., 2016). In the twin-jet spectra, a distinct new peak was
215 observed at position 880 cm^{-1} at 55 K, which was likely to be attributed to the C3-CIs. The resulting ~ 7 cm^{-1} deviation might be attributable to the Ar matrix effect (Bach, 1999). The calculated O-O stretching vibrations of C7-CIs were located at 882 (syn-C7-CIs) and 910 (anti-C7-CIs) cm^{-1} . According to Table S1, the calculated IR peaks of CIs were consistently overestimated by over 10 cm^{-1} relative to experimental values, with the deviation being most pronounced for anti-CIs. Notably, no distinct new peaks appeared below 882 cm^{-1} in the experiment. This absence suggested that very few stabilized C7-CIs were likely generated during the ozonolysis of myrcene. Instead, most C7-CIs were consumed via unimolecular decay pathways, this conclusion which was also supported by our subsequent analysis. ~~The calculated O-O stretching vibrations of C7-CIs were located at 892 (syn C7-CIs) and 923 (anti C7-CIs) cm^{-1} , which were covered by the main characteristic infrared vibration peaks of myrcene. Consequently, it was challenging to directly observe the strongest characteristic infrared vibration peaks belonging to C7-CIs. In addition to the -COO group, C7-CIs also possessed conjugated double bonds as characteristic functional groups. In both syn and anti C7-CIs, the second most intense infrared vibration band consistently corresponded to the wagging vibration of the =CH₂ group on the conjugated moiety. The calculated position of this vibration agreed with that of myrcene. Position 905 cm^{-1} was the infrared characteristic peak generated by the wagging vibration of myrcene =CH₂, as obtained by twin jet method. In the spectra, a significant relative increase at the 905 cm^{-1} position was observed after annealing~~
220
225

to 55 K. This increase might be attributable to the generation of C7-CIs. The characteristic infrared peaks of C3- and C7-CIs were both generated after 55 K annealing.

In addition to the early intermediates, acetone was also identified as a major product co-produced with C7-CIs in myrcene ozonolysis. The spectral bands of 1370 and 1720 cm^{-1} appeared in the twin-jet spectra belong to acetone (Han and Kim, 1996). The generation of acetone also indirectly demonstrated the formation of C7-CIs. The peak at 905 cm^{-1} coincided in temperature with the C3-CIs peaks and suggested its assignment to the =CH₂ wagging vibration of the C7-aldehyde. MI-FTIR experiments unequivocally verified that myrcene ozonolysis proceeded via the Criegee mechanism. Furthermore, both C3- and C7- CIs were generated during this process.

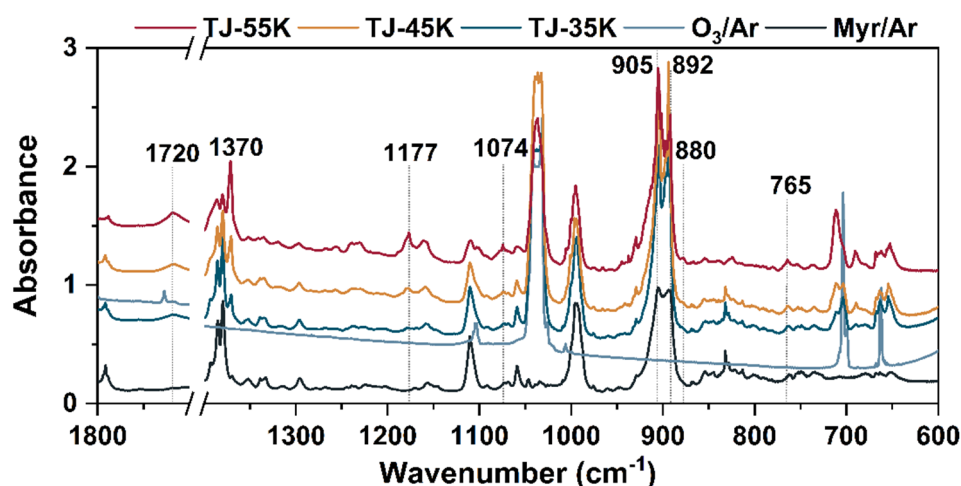


Figure 2 The twin-jet IR spectra of myrcene ozonolysis reaction in a low temperature and Ar matrix after annealing to 35 K, 45 K and 55 K. The blank spectra of myrcene/Ar and O₃/Ar were also given. T-J means the spectra obtained by twin-jet method.

Table 12 Identification and assignments of experimental absorption bands in the initial ozonolysis of myrcene.

Experimental bands/(cm^{-1})	Calculated Band/(cm^{-1})	Reference	Belonger	Assignment
765	\	772	POZs	O-O-O str.
880	\	887 ^a	C3-CIs	O-O str.
905	\	\	<u>4-vinyl-4-pentene</u> C7-CIs	=CH ₂ wag.
1074	105468	\	POZs	C-O str.
1177	116574	\	POZs	C-O str.
1370	\	1370 ^b	Acetone	δ CH ₃
1720	\	1721.6 ^b	Acetone	C=O str.

Note: ^a The characteristic infrared peaks of gas-phase C3-CIs measured by step-scanning Fourier transform infrared spectroscopy (Wang et al., 2016).

^b Measure in the low- temperature Ar matrices (Han and Kim, 1996).

^c str. stands for stretching vibration; wag. stands for wagging vibration; δ stands for the scissoring vibration.

3.2 Impact of CIs on SOA generation

To explore the contribution of CIs to the SOA generation, the myrcene ozonolysis experiments were conducted under different conditions— (with or without an OH scavenger and at varying RH levels) in a 1.2 m³ smog chamber (Table 2). The unimolecular decay of both excited CIs and SCIs could produce OH radical. Therefore, SOA formation included contributions

from both SCIs and OH radical derived in myrcene ozonolysis.

250 As shown in Table 2, Exp. 1-2 added n-hexane (HA) as an OH radical scavenger to highlight the contribution of SCIs-derived pathways. Exp. 3-5 were conducted with progressively increasing RH to modulate SOA formation by introducing direct reactions between water and SCIs. The volume concentration of the particles rose sharply within approximately 30 minutes and reached its maximum value within 180 minutes (Figure S2). The dominant size range of SOA expanded from 50-250 nm during myrcene ozonolysis (Figure 3). The suppression of particle formation induced by the OH scavenger and elevated RH

255 was conspicuously demonstrated. Following the 367 ppm HA addition, the particle yield from myrcene ozonolysis decreased by approximately 72%. As RH increased from dry conditions to ~20% and subsequently to 50%, the particle yield gradually declined by 17% to 40% (Table 2). As shown in Fig. 32(a), after the addition of HA, no significant reduction in the particle size distribution was observed within the first 30 min. This might be attributed to the rapid reactions of SCIs, indicating that gas-phase reactions of SCIs played an important role in particle nucleation. Between 90 and 180 min of reaction, the particle

260 size distribution decreased markedly. This reduction was due to the scavenging of OH radicals, which inhibited the formation of OH-RO₂ pathway. Bimolecular reactions and the autoxidation of OH-RO₂ played a crucial role in the growth of SOA (Baker et al., 2024). As the RH gradually increased from ~20% to 50%, the growth of particle size was inhibited across different time periods. This phenomenon occurred because reactions between water and SCIs might prevent these compounds from converting into larger, less volatile products. Therefore, OH radical generated from CIs and SCIs also contributed to the growth

265 of particle size distribution and enhanced SOA yield.

Table 2 Summary of experimental conditions.

Exp.	[Myrcene]/ppb	[O ₃]/ppb	RH/%	Scavenger	M _{SOA} (μg/cm ³)	Y _{SOA}
1	171.5	~ 200	< 0.5	/	346	0.36
2	170	~ 200	< 0.5	~ 367 ppm HA	91	0.10
3	222	~ 200	< 0.5	/	509	0.41
4	231	~ 200	~20	/	432	0.34
5	230	~ 200	~50	/	311	0.24

Note: n-hexane is abbreviated as HA.

The O₃ concentration listed in the table is the value recorded after the O₃ analyzer stabilized for 20 minutes, which corresponds to the 20-minute mark after the initiation of the experiment.

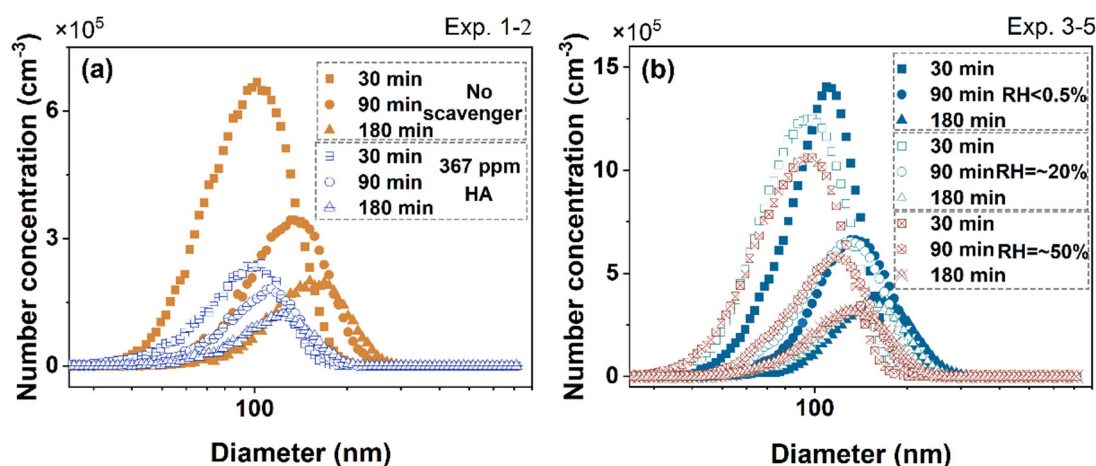


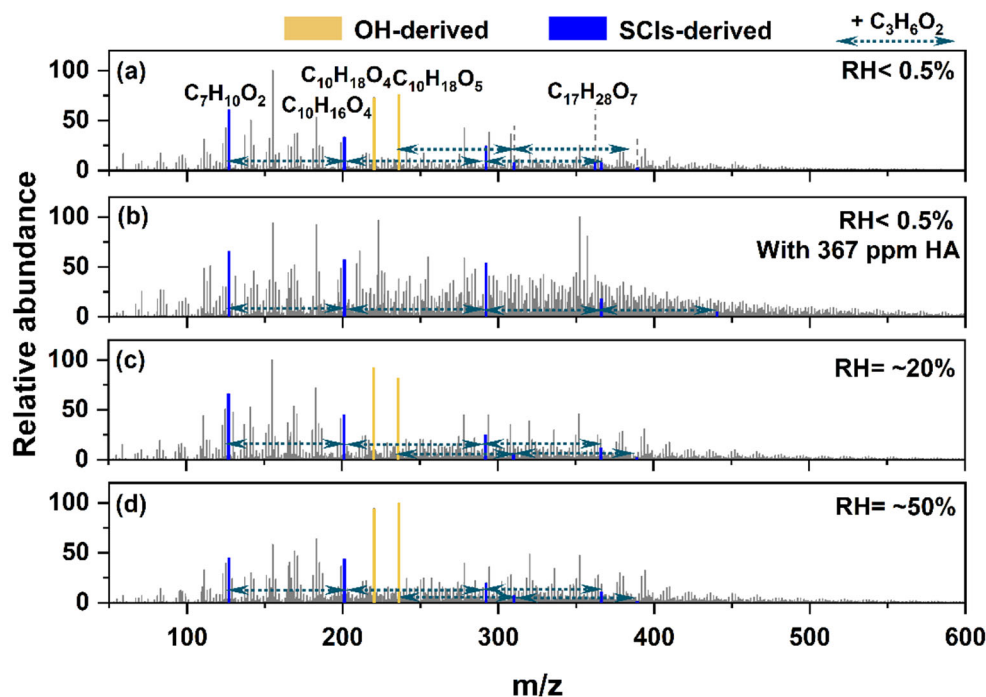
Figure 3 Time series of size distributions of aerosol particles formed at 30, 90, and 180 min after the initiation of myrcene ozonolysis under different conditions. (a) depicted particle formation processes corresponding Exp. 1-2 from Table 2, while (b) illustrated particle formation processes in Exp. 3-5 from Table 2.

3.3 Mechanism of SCIs contribution to SOA

UHPLC-ESI-MS was employed to analyze the chemical compositions of SOA collected offline. CIs were important SOA precursors during the ozonolysis process. In this study, the contribution mechanisms of CIs to SOA formation were proposed in myrcene ozonolysis.

C₁₀H₁₈O₅ and C₁₀H₁₈O₄, with relative abundances (RA) of 76% and 73% respectively, ranked among the top 3 in the absence of any scavengers at RH < 0.5% as shown in Figure 4(a). The formation of these two intense peaks was belonged to the contribution of OH radical oxidation processes. The OH radical was almost entirely originated from the CIs unimolecular decomposition/ degradation reactions. The OH radical and O₂ reacted sequentially with myrcene to form C₁₀H₁₇O₃ radical (C₁₀-R₂O₂·) as shown in Scheme-Figure 1, R6). C₁₀H₁₇O₃ radical then underwent autoxidation channel which was highly likely to occur to produce C₁₀H₁₇O₅ radical (C₁₀-R₂O₂·) (Jokinen et al., 2014). The reaction of C₁₀H₁₇O₅ radical with HO₂ yielded C₁₀H₁₈O₅ (C₁₀-R₂OOH) which was detected as the main product. Meanwhile, C₁₀H₁₇O₅ radical could also react with any RO₂ radical to yield C₁₀H₁₈O₄ (C₁₀-R₂OH). The relative peak intensity of C₇H₁₀O₂ was slightly lower than that of C₁₀H₁₈O₅ and C₁₀H₁₈O₄, and its molecular formula was consistent with C7-CIs. It was inferred that it might originate from C7-OH produced

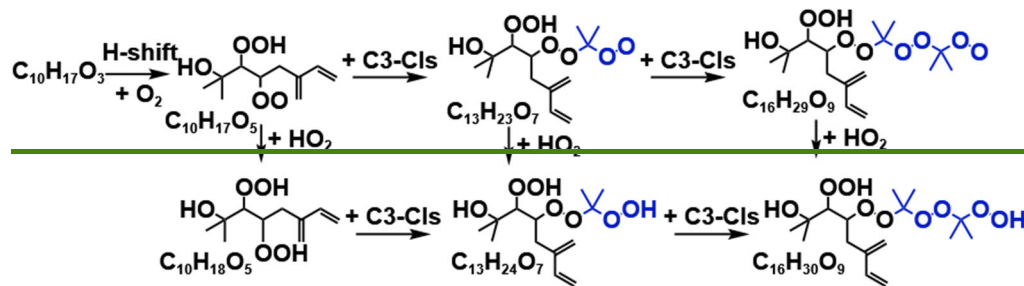
290 during the unimolecular decomposition/degredation of C7-CIs. C7-CIs underwent unimolecular decomposition/degredation via the VHP pathway, producing OH radical while simultaneously generating R radical. The R radical subsequently reacted with O₂ to form C₇H₉O₃-(C7-RO₂). C₇H₉O₃ could react with any RO₂ radical to form C₇H₁₀O₂ (C7-OH). The OH radical yield from myrcene ozonolysis was generally high, which also confirmed that the larger CIs generated during this process tend to react via unimolecular decay pathways (Cox et al., 2020).

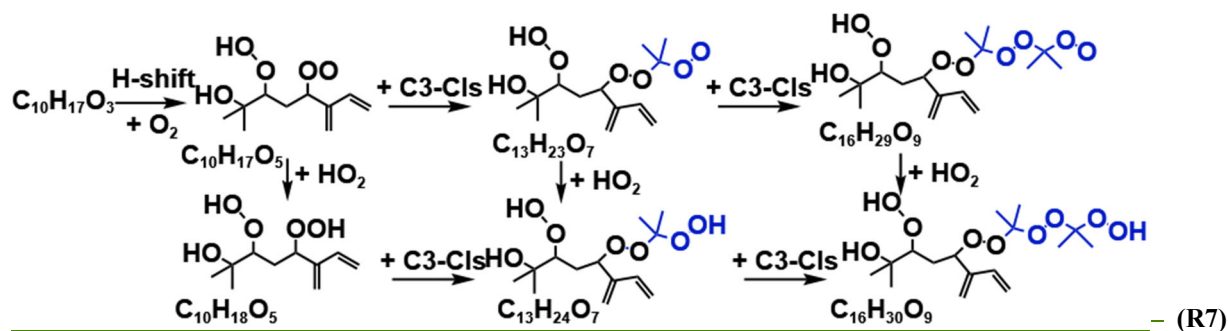


295 **Figure 4** UHPLC/ESI-MS of SOA from myrcene ozonolysis in different conditions. (a) No scavenger was added. (b) 367 ppm *n*-hexane (HA) was added. (c) RH~20% condition. (d) RH~50% condition. The substances marked by the yellow lines originated from the OH-derived channel, while those marked by the blue lines mainly originated from the SCIs-derives channel. The oligomer sequence containing C3-CIs as the chain unit was marked by the green dotted line.

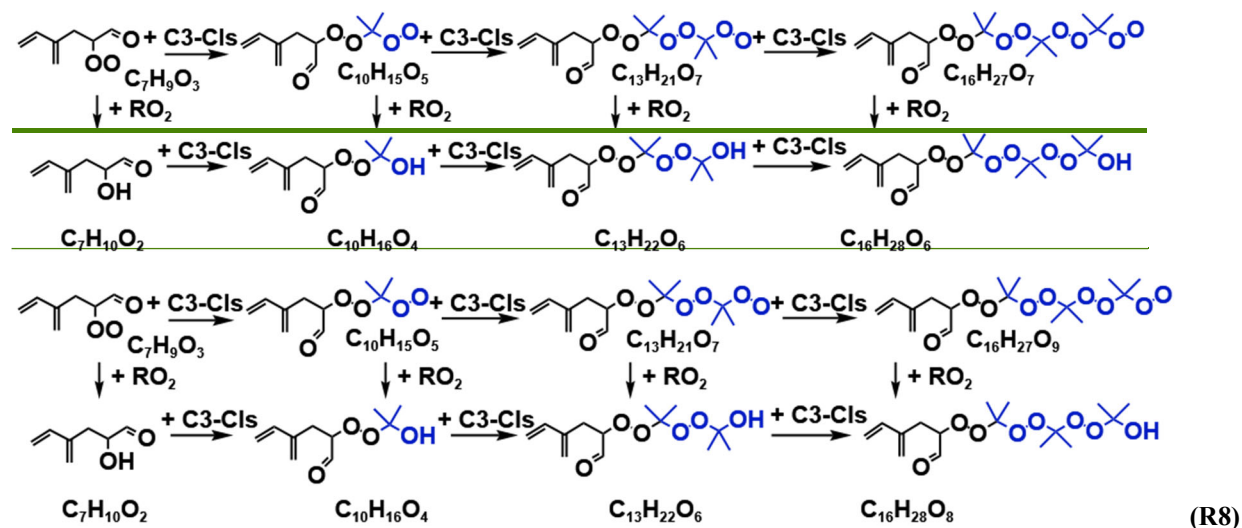
300 C₁₀H₁₇O₅ radical as the main RO₂ radical could undergo sequential oligomerization. Several peaks representing ordered oligomers with C₃H₆O₂ as chain units were found. The chemical formula of C₃H₆O₂ was identical to C3-CIs and confirmed to exist by the matrix isolation experiment. The proposed pathway was shown in R7. The rate constants for the reaction of RO₂ radicals with SCIs were much higher than that for ROOH (Zhao et al., 2017; Chao et al., 2024; Chhantyal-Pun et al., 2020; Caravan et al., 2024). C₁₀H₁₇O₅ radical reacted with one or two C3-CIs, followed by reaction with HO₂ radical resulting in chain termination (C₁₀H₁₇O₅ + n C3-CIs + HO₂, n= 0-2, Sequence 1). However, the relative intensities of this set of oligomer signals were relatively low. This was likely because C₁₀H₁₇O₅ radical more readily reacted with HO₂ or RO₂ to form C₁₀H₁₈O₅ and C₁₀H₁₈O₄, thereby reducing the likelihood of its reaction with C3-CIs in the gas phase. These oligomer sequences exhibited similar distribution patterns of major fragment ion peaks in MS/MS spectra in Figure S3(a). Therefore, these oligomers with C3-CIs as the chain units had similar structural units in their chemical composition. Moreover, the corresponding structural assignments for its major fragment peaks were provided in Figure S3(b). The fragments C₅H₇⁺ (m/z 67.06), C₆H₉O₂⁺ (m/z 113.06), and C₉H₁₃O⁺ (m/z 137.10) revealed that the oligomers in Sequence 2-1 all feature a carbon chain skeleton characterized by conjugated double bonds. The C₃H₇O⁺ (m/z 59.05)/C₃H₇O₂⁺ (m/z 75.05) fragment ions originated from cleavage of terminal

-OH or -OOH functionalized tertiary carbon moieties in the oligomers. For C7-CIs, no significant oligomers with C7-CIs as chain units were observed when reacting with C₁₀H₁₇O₅ radical. Although the mass spectral peak corresponding to C₁₇H₂₈O₇ was observed and its molecular formula aligned with the expected product of C₁₀H₁₇O₅ + C7-CIs. But C₁₇H₂₈O₇ could also originate from C₁₀H₁₇O₅ + C7-RO₂H₁₁O₄ (C₇H₁₁O₄) the formation pathway as shown in Scheme S1). Moreover, C₁₇H₂₈O₇ was classified as a low-volatility organic compound (LVOCs) (Donahue et al., 2012; Donahue et al., 2011), which readily partitioned into the particle phase. But its low abundance implied C₁₇H₂₈O₇ did not appear as a dominant product in the mass spectra. Consequently, the contribution of C7-CIs oligomerization to myrcene-derived SOA formation might be considered negligible. In addition, an ordered oligomer sequence formed by C₇H₁₀O₂ + n C3-CIs was also identified. The corresponding compounds in the sequence are C₇H₁₀O₂ (m/z 127.075), C₁₀H₁₆O₄ (m/z 201.112), C₁₃H₂₂O₆ (m/z 292.175) and C₁₆H₂₈O₈ (m/z 371.168), namely Sequence 2 (The peaks with relative abundance of less than 1% were ignored). The proposed pathway of Sequence 2 was as shown in the R8. Sequence 2 had a greater degree of oligomerization and contributed more to particle formation than Sequence 1. This indicated that C₇H₉O₃, which produced by C7-CIs unimolecular reaction, more readily reacted with C3-CIs in the gas phase. The oligomerization reactions within the Sequence 2 all terminated with the reaction of RO₂ radical (C₇H₉O₃ + n C3-CIs + RO₂). Figure S4 presented the MS/MS spectrum of Sequence 2 along with the proposed structures corresponding to the major fragment peaks. The presence of fragments such as C₅H₇⁺ (m/z 67.06), C₇H₇O⁺ (m/z 95.05), and C₆H₉O₂⁺ (m/z 113.06) indicated that the oligomers in Sequence 2 possessed a conjugated double-bond skeleton. This suggested that this sequence was initiated by C7 compounds. The fragment at m/z 71.05 (C₄H₇O⁺) was generated via α-cleavage adjacent to a carbonyl group in the oligomer backbone. This fragmentation was typical of compounds containing conjugated carbonyl motifs and further supported the presence of a C7-based conjugated skeleton in the sequence. The C₃H₇O⁺ (m/z 59.05) fragment ions originated from cleavage of terminal -OH functionalized tertiary carbon moieties in the oligomers. The formation of this ion fragment was similar to that in Sequence 1. In the MS/MS spectra of C₁₀H₁₆O₄, we observed that besides the fragment peaks annotated in Figure S4, there existed fragment ion peaks with higher intensities. This suggested that C₁₀H₁₆O₄ was formed through multiple pathways (such as the RO₂ + RO₂ reaction) (Peräkylä et al., 2023; Frandsen et al., 2025). Consistently, no discernible oligomerization signals were detected for reactions using C₇H₉O₃ as the starting reactant with C7-CIs.



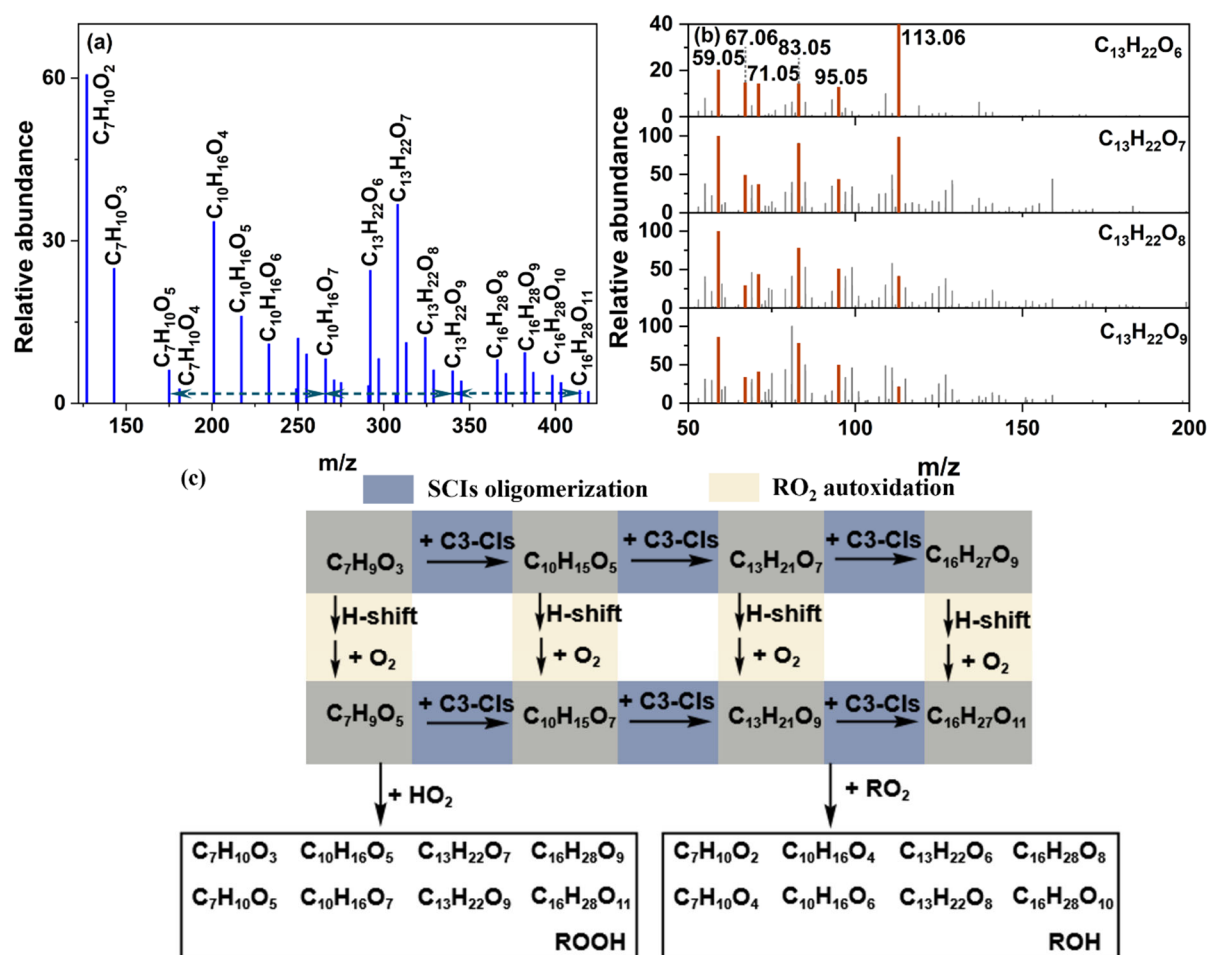


340 As shown in Figure 4(b), the peaks corresponding to $C_{10}H_{18}O_4$ and $C_{10}H_{18}O_5$ disappeared after the addition of the OH radical scavenger, as expected. The $C_7H_{10}O_2$ peak remained, which further demonstrated that $C_7H_{10}O_2$ originated from SCIs-derived products. Compared with the mass spectrum without the scavenger, the contribution of the oligomers in Sequence 2 markedly increased. Following the introduction of the scavenger, the peak intensities corresponding to compounds with higher degrees of oligomerization ($C_{13}H_{22}O_6$ and $C_{16}H_{28}O_8$) within the sequence were significantly enhanced. Moreover, compared to the spectrum acquired in the absence of the scavenger, a more highly oligomerized compound ($C_{19}H_{34}O_{10}$) was detected. Water served as the dominant removal pathway for SCIs in the atmosphere. Correspondingly, the contribution of Sequence 2 to SOA formation decreased progressively with increasing RH as shown in Figure 4(c) and (d), especially substances with a higher degree of oligomerization in the sequence ($C_{13}H_{22}O_6$ and $C_{16}H_{28}O_8$). So, the Sequence 2 was primarily contributed by SCIs-derived.



350 Meanwhile, some compounds were found to have the same number of C and H atoms, differing only in the number of O atoms in parallel oligomer sequences, namely, $C_7H_{10}O_{2-5}$, $C_{10}H_{16}O_{4-7}$, $C_{13}H_{22}O_{6-9}$ and $C_{16}H_{28}O_{8-11}$ (Sequence 2N) as shown in Figure 5(a). Compounds with identical carbon and hydrogen atom counts exhibited closely resembling major fragment ions in their MS/MS spectra as shown in Figure 5(b). This suggested that compounds with identical carbon and hydrogen atom counts exhibited highly consistent formation pathways. The process leading to progressive oxygenation (i.e., increasing oxygen atom content) was the RO_2 autoxidation mechanism (Jokinen et al., 2014; Liu et al., 2023). Simultaneously, Sequence 2N was the oligomer series formed by oligomerization with C3-ClIs as chain units. This indicated that SCIs oligomerization and RO_2 autoxidation mechanistically interplayed in the formation of Sequence 2N. The proposed formation mechanism of Sequence

360 2N was illustrated in Figure 5(c). RO₂ underwent oligomerization with n SCIs to form the oligomer RO₂-n SCIs, while concurrently undergoing autoxidation to generate R'O₂. R'O₂ might subsequently underwent analogous cycles of SCIs oligomerization and autoxidation. This radical propagation cascade ultimately terminated via reactions with RO₂ or HO₂ radical. SCIs inherently contained at least two oxygen atoms in their structure due to the presence of terminal -COO groups. The RO₂ autoxidation inherently involved reaction with O₂, which rapidly elevated the oxygen content in products. Consequently, the synergistic interplay between SCIs oligomerization and RO₂ autoxidation facilitated rapid formation of high-molecular-weight species and highly oxygenated molecules (HOMs), which substantially contributed to particle nucleation and growth.



370 **Figure 5** The relative abundance and the proposed **mechanism pathways** of oligomer sequences derived from the synergistic SCIs oligomerization and RO₂ autoxidation. (a) Mass spectrometric distribution of oligomeric sequences under dry conditions. (b) The MS/MS spectra of C₁₃H₂₂O₆₋₉ and the major fragment ions were highlighted in orange in the mass spectra. (c) The proposed mechanism of this oligomer sequences. The blue area denoted the SCIs oligomerization pathway. The yellow area represented the RO₂ autoxidation pathway. The black solid box indicated the particulate composition detected by mass spectrometry (MS).

The addition of different scavengers also affected the formation of Sequences 2N. Figure 6 illustrated the proportions of compounds with various oligomerization degrees of oligomerization in Sequence 2N under different scavenger conditions. The dominant compounds in Sequences 2N were C₁₃H₂₂O₆₋₉ which contained two C3-CIs as chain units under dry conditions, with or without added OH radical (Figure 6(a) and (b)). Furthermore, following the addition of OH radical, the proportions of both C₁₃H₂₂O₆₋₉ and C₁₆H₂₈O₈₋₁₁ in Sequences 2N gradually increased (Figure 6(b)). This indicated that the SCIs oligomerization reaction significantly contributed to the particle formation after the addition of the OH scavenger. This was

380 consistent with the result observed in Sequences 2. As the RH increased, the main compound in Sequences 2N became $C_{10}H_{16}O_{4-7}$, which contained only a single C3-CIs as a chain unit (Figure 6(c) and (d)). The proportions of both $C_{13}H_{22}O_{6-9}$ and $C_{16}H_{28}O_{8-11}$ in Sequence 2N decreased with increasing RH. This indicated that the reaction of water with C3-CIs directly affected the generation of oligomers with higher degrees of oligomerization. Additionally, the fraction of $C_7H_{10}O_{2-5}$ decreased significantly with increasing RH. This indicated that besides reacting with C3-CIs, water also scavenged C7-CIs to some extent. Therefore, the contribution of the SCIs oligomerization mechanism to SOA formation were suppressed under elevated RH

385 conditions.

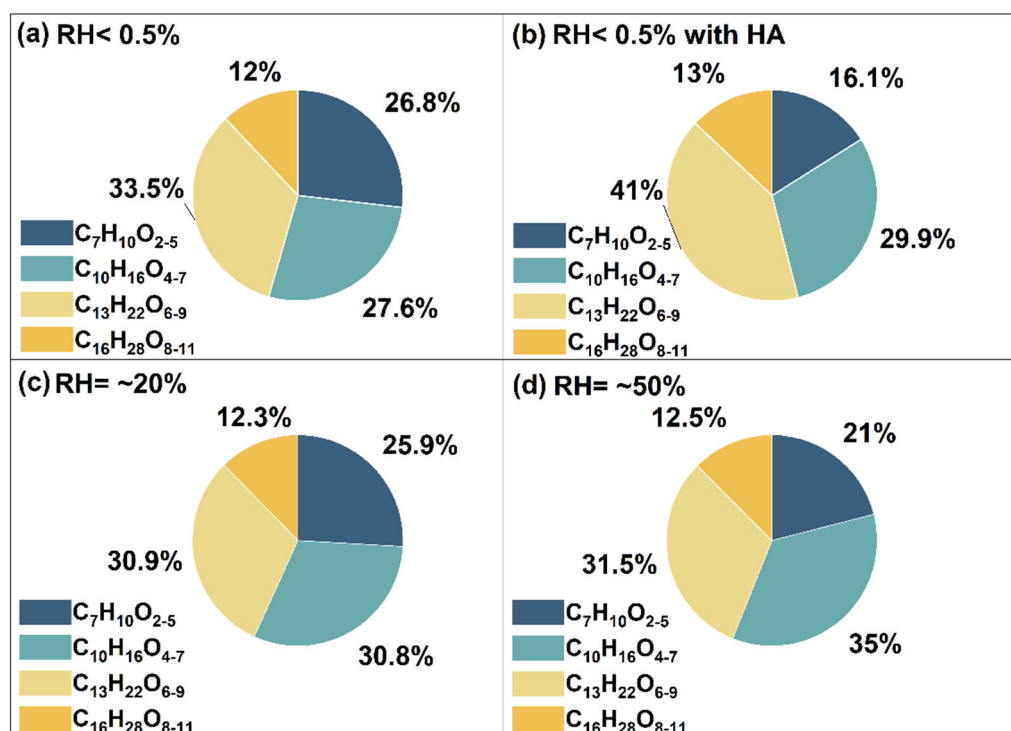


Figure 6 The proportion of compounds in sequence 2N generated during the myrcene ozonolysis under different conditions.

Sequence 1, 2 and 2N demonstrated ordered oligomers formed with C3-CIs as chain units. However, ordered oligomeric sequences ($RO_2 + n$ C7-CIs + HO_2/RO_2 , $n \geq 2$) with C7-CIs as the chain unit were not discovered. Based on the current formation

390 mechanism of oligomers, C3-CIs and C7-CIs differed in their contribution to particle formation in myrcene ozonolysis. For smaller molecular-sized CIs (C3-CIs), the primary pathway for partitioning into the particle involved oligomerization with RO_2 radical and other species. The C7-CIs had higher molecular masses than C3-CIs. The products from unimolecular and bimolecular reaction of C7-CIs partitioned more readily to particles which reduced the viability to function as chain units in oligomerization processes (Donahue et al., 2012; Donahue et al., 2011). Furthermore, C7- RO_2 generated from unimolecular

395 decomposition of C7-CIs acts as a chain-initiating precursor that reacts with C3-CIs, thereby contributing to particle nucleation. These findings implied divergent dominant pathways for SOA formation mediated by SCIs across varying molecular dimensions in VOCs ozonolysis. The C10-CIs with high molecular weights generated during the ozonolysis of α -pinene and limonene might also be more likely to incorporate into the particle via unimolecular reaction mechanisms rather than through

oligomerization. Our findings further demonstrated that when evaluating SCIs contribution pathways to SOA, the molecular size of SCIs ~~must~~ might be prioritized especially during monoterpene ozonolysis. The molecular size of SCIs might lead to differences in their primary mechanisms of contributing to SOA formation. In the myrcene ozonolysis system, the branching ratio might favor the formation of C3-CIs over C7-CIs, which further enhanced the propensity of C3-CIs toward oligomerization. Currently, no literature has elucidated the contribution mechanisms of CIs of different sizes to SOA formation from the perspective of molecular size. This study presented this concept for the first time.

4. Conclusions

This study employed the MI-FTIR method to determine the presence of C3-CIs and C7-CIs during the myrcene ozonolysis. The O-O stretching vibration peak of C3-CIs was located at 880 cm⁻¹. The absence of characteristic infrared peaks belonged to C7-CIs, likely due to their low steady-state yield or rapid unimolecular decay. The characteristic IR peaks of acetone indirectly confirmed the production of C7-CIs.

~~This study employed the MI-FTIR method to directly determine the presence of C3-CIs and C7-CIs during the myrcene ozonolysis. The O-O stretching vibration peak of C3-CIs was located at 880 cm⁻¹. The characteristic infrared vibration peak of C7-CIs, caused by the =CH₂ wagging vibration on the conjugated double bonds, was located at 905 cm⁻¹.~~

Furthermore, combined with smog chamber experiments, it was verified that these two distinct CIs of different molecular sizes differ in their primary contribution mechanisms during SOA formation. For C3-CIs, they primarily underwent oligomerization reactions (e.g., RO₂ + n C3-CIs + RO₂/HO₂) to form lower-volatility oligomers that incorporate into the particle. Meanwhile, the SCIs oligomerization and RO₂ autoxidation synergistically occurred during the myrcene ozonolysis, leading to the formation of HOMs-RO₂ with higher oxygen content. To our knowledge, this was the first time this synergistic ~~mechanism effect~~ effect has been proposed. Larger C7-CIs primarily underwent unimolecular decomposition, producing C7-ROH and C7-RO₂. C7-ROH could be detected as a stable product in particle. The C7-RO₂ subsequently oligomerized with n C3-CIs to partition into the particle phase. The coexistence of carbon atoms with varying molecular sizes leads to a different role of CIs in secondary organic aerosol SOA formation during the ozonolysis of myrcene, compared to that observed in cyclic monoterpenes (e.g., α-pinene and limonene). The structural similarity of ocimene to myrcene meant its ozonolysis might also lead to CIs of varying sizes, potentially allowing for this synergistic effect. ~~The coexistence of these CIs of different molecular sizes led to a distinctly different ozonolysis mechanism for myrcene compared to that of cyclic monoterpenes (e.g., α-pinene, limonene).~~ An increase in RH caused some SCIs to react directly with water, thereby reducing the fraction of SCIs that form oligomers and partition into the particle. This mechanism also significantly contributed to the decrease in SOA yield and the shift toward a smaller particle size distribution. Our study further deepened the understanding of monoterpene ozonolysis mechanisms, particularly from the perspective of Criegee chemistry.

Data availability

430 All raw data can be provided by the corresponding authors upon request.

Supplement

The supplement related to this article is available online at:

Author contribution

MFC and SRT planned the campaign; MFC, XFL and YYX performed the measurements; MFC and SSY analyzed the data;
435 MFC wrote the manuscript draft; MFC, SRT, SST, HLZ and MFG reviewed and edited the manuscript.

Competing interests

The authors declare that they have no conflict of interest.

Acknowledge

This work was supported by the National Key Research and Development Program of China (No. 2022YFC3700200), National
440 Natural Science Foundation of China (Contract No. 42130606), Beijing National Laboratory for Molecular Sciences (BNLMS-
CXXM-202011).

References

- Anglada, J. M. and Sole, A.: Impact of the water dimer on the atmospheric reactivity of carbonyl oxides, *Phys. Chem. Chem. Phys.*, 18, 17698-17712, 10.1039/c6cp02531e, 2016.
- 445 Aschmann, S. M., Arey, J., and Atkinson, R.: OH radical formation from the gas-phase reactions of O₃ with a series of terpenes, *Atmos. Environ.*, 36, 4347-4355, 10.1016/s1352-2310(02)00355-2, 2002.
- Atkinson, R., Hasegawa, D., and Aschmann, S. M.: Rate constants for the gas-phase reactions of O₃ with a series of monoterpenes and related-compounds at 296±2 K, *Int. J. Chem. Kinet.*, 22, 871-887, 10.1002/kin.550220807, 1990.
- Bach, S. B. H.: *Matrix-Isolation Techniques: A Practical Approach*. The Practical Approach in Chemistry Series By Ian R. Dunkin (University of Strathclyde). Oxford Press: New York. 1998. 242 pp. \$105.00. ISBN 0-19-855863-5, *J. Am. Chem. Soc.*, 121, 5618-5618, 10.1021/ja9857099, 1999.
- 450 Baker, Y., Kang, S., Wang, H., Wu, R., Xu, J., Zanders, A., He, Q., Hohaus, T., Ziehm, T., Geretti, V., Bannan, T. J., O'Meara, S. P., Voliotis, A., Hallquist, M., McFiggans, G., Zorn, S. R., Wahner, A., and Mentel, T. F.: Impact of HO₂/RO₂ ratio on highly

- oxygenated α -pinene photooxidation products and secondary organic aerosol formation potential, *Atmos. Chem. Phys.*, 24, 4789-4807, 10.5194/acp-24-4789-2024, 2024.
- 455 Boge, O., Mutzel, A., Iinuma, Y., Yli-Pirila, P., Kahnt, A., Joutsensaari, J., and Herrmann, H.: Gas-phase products and secondary organic aerosol formation from the ozonolysis and photooxidation of myrcene, *Atmos. Environ.*, 79, 553-560, 10.1016/j.atmosenv.2013.07.034, 2013.
- Boy, M., Mogensen, D., Smolander, S., Zhou, L., Nieminen, T., Paasonen, P., Plass-Dulmer, C., Sipila, M., Petaja, T., Mauldin, 460 L., Berresheim, H., and Kulmala, M.: Oxidation of SO₂ by stabilized Criegee intermediate (sCI) radicals as a crucial source for atmospheric sulfuric acid concentrations, *Atmos. Chem. Phys.*, 13, 3865-3879, 10.5194/acp-13-3865-2013, 2013.
- Caravan, R. L., Bannan, T. J., Winiberg, F. A. F., Khan, M. A. H., Rousso, A. C., Jasper, A. W., Worrall, S. D., Bacak, A., Artaxo, P., Brito, J., Priestley, M., Allan, J. D., Coe, H., Ju, Y., Osborn, D. L., Hansen, N., Klippenstein, S. J., Shallcross, D. E., Taatjes, C. A., and Percival, C. J.: Observational evidence for Criegee intermediate oligomerization reactions relevant to 465 aerosol formation in the troposphere, *Nat. Geosci.*, 17, 219–226, 10.1038/s41561-023-01361-6, 2024.
- [Chao, W., Markus, C. R., Okumura, M., Winiberg, F. A. F., and Percival, C. J.: Chemical Kinetic Study of the Reaction of CH₂OO with CH₃O₂, *Journal of Physical Chemistry Letters*, 15, 3690-3697, 10.1021/acs.jpcclett.4c00159, 2024.](#)
- Chen, L., Huang, Y., Xue, Y. G., Jia, Z. H., and Wang, W. L.: Oligomer formation from the gas-phase reactions of Criegee intermediates with hydroperoxide esters: mechanism and kinetics, *Atmos. Chem. Phys.*, 22, 14529-14546, 10.5194/acp-22- 470 14529-2022, 2022.
- Chen, L., Huang, Y., Xue, Y., Shen, Z., Cao, J., and Wang, W.: Mechanistic and kinetics investigations of oligomer formation from Criegee intermediate reactions with hydroxyalkyl hydroperoxides, *Atmos. Chem. Phys.*, 19, 4075-4091, 10.5194/acp-19- 4075-2019, 2019.
- Chen, M. F., Tong, S. R., Yu, S. S., Xu, Y. Y., Lv, X. F., Zhang, H. L., Wang, S. F., and Ge, M. F.: Impact of the Criegee 475 Intermediate on the Formation of Secondary Organic Aerosols during E-4-Hexen-1-ol Ozonolysis, *J. Phys. Chem. A*, 129, 1704-1713, 10.1021/acs.jpca.4c08028, 2025.
- Chen, M. F., Tong, S. R., Wang, Z., Li, W. R., Xu, Y. Y., Wang, S. F., and Ge, M. F.: Reaction mechanism and kinetics of Criegee intermediate and hydroperoxymethyl formate, *J. Environ. Sci.*, 105, 128-137, 10.1016/j.jes.2020.12.029, 2021.
- [Chen, T., Zhang, P., Chu, B., Ma, Q., Ge, Y., Liu, J., and He, H.: Secondary organic aerosol formation from mixed volatile 480 organic compounds: Effect of RO₂ chemistry and precursor concentration, *Npj Clim. Atmos. Sci.*, 5, 95, 10.1038/s41612-022-00321-y, 2022.](#)
- Chhantyal-Pun, R., Davey, A., Shallcross, D. E., Percival, C. J., and Orr-Ewing, A. J.: A kinetic study of the CH₂OO Criegee intermediate self-reaction, reaction with SO₂ and unimolecular reaction using cavity ring-down spectroscopy, *Phys. Chem. Chem. Phys.*, 17, 3617-3626, 10.1039/c4cp04198d, 2015.
- 485 Chhantyal-Pun, R., Khan, M. A. H., Zachhuber, N., Percival, C. J., Shallcross, D. E., and Orr-Ewing, A. J.: Impact of Criegee

Intermediate Reactions with Peroxy Radicals on Tropospheric Organic Aerosol, *Acs Earth Space Chem.*, 4, 1743-1755, 10.1021/acsearthspacechem.0c00147, 2020.

Cox, R. A., Ammann, M., Crowley, J. N., Herrmann, H., Jenkin, M. E., McNeill, V. F., Mellouki, A., Troe, J., and Wallington, T. J.: Evaluated kinetic and photochemical data for atmospheric chemistry: Volume VII - Criegee intermediates, *Atmos. Chem. Phys.*, 2020, 13497-13519, 10.5194/acp-2020-472, 2020.

Criegee, R.: Mechanism of Ozonolysis, *Angew. Chem. Int. Edit.*, 14, 745-752, <https://doi.org/10.1002/anie.197507451>, 1975.

Deng, P., Wang, L., and Wang, L.: Mechanism of Gas-Phase Ozonolysis of β -Myrcene in the Atmosphere, *J. Phys. Chem. A*, 122, 3013-3020, 10.1021/acs.jpca.8b00983, 2018.

Donahue, N. M., Epstein, S. A., Pandis, S. N., and Robinson, A. L.: A two-dimensional volatility basis set: 1. organic-aerosol mixing thermodynamics, *Atmos. Chem. Phys.*, 11, 3303-3318, 10.5194/acp-11-3303-2011, 2011.

Donahue, N. M., Kroll, J. H., Pandis, S. N., and Robinson, A. L.: A two-dimensional volatility basis set - Part 2: Diagnostics of organic-aerosol evolution, *Atmos. Chem. Phys.*, 12, 615-634, 10.5194/acp-12-615-2012, 2012.

[Frandsen, B. N., Franzon, L., Meder, M., Pasik, D., Ahongshangbam, E., Vinkvist, N., Myllys, N., Iyer, S., Rissanen, M. P., Ehn, M., and Kurtén, T. C.: Detailed Investigation of 2,3-Dimethyl-2-butene Ozonolysis-Derived Hydroxyl, Peroxy, and Alkoxy Radical Chemistry, *ACS Earth Space Chem.*, 9, 1322-1337, 10.1021/acsearthspacechem.4c00355, 2025.](#)

Frisch, M. J., Trucks, G. W., Schlegel, H. B., Scuseria, G. E., Robb, M. A., Cheeseman, J. R., Scalmani, G., Barone, V., Petersson, G. A., Nakatsuji, H., Li, X., Caricato, M., Marenich, A. V., Bloino, J., Janesko, B. G., Gomperts, R., Mennucci, B., Hratchian, H. P., Ortiz, J. V., Izmaylov, A. F., Sonnenberg, J. L., Williams, Ding, F., Lipparini, F., Egidi, F., Goings, J., Peng, B., Petrone, A., Henderson, T., Ranasinghe, D., Zakrzewski, V. G., Gao, J., Rega, N., Zheng, G., Liang, W., Hada, M., Ehara, M., Toyota, K., Fukuda, R., Hasegawa, J., Ishida, M., Nakajima, T., Honda, Y., Kitao, O., Nakai, H., Vreven, T., Throssell, K., Montgomery Jr., J. A., Peralta, J. E., Ogliaro, F., Bearpark, M. J., Heyd, J. J., Brothers, E. N., Kudin, K. N., Staroverov, V. N., Keith, T. A., Kobayashi, R., Normand, J., Raghavachari, K., Rendell, A. P., Burant, J. C., Iyengar, S. S., Tomasi, J., Cossi, M., Millam, J. M., Klene, M., Adamo, C., Cammi, R., Ochterski, J. W., Martin, R. L., Morokuma, K., Farkas, O., Foresman, J. B., and Fox, D. J.: *Gaussian 16 Rev. A.03*, 2016.

Gong, Y. W. and Chen, Z. M.: Quantification of the role of stabilized Criegee intermediates in the formation of aerosols in limonene ozonolysis, *Atmos. Chem. Phys.*, 21, 813-829, 10.5194/acp-21-813-2021, 2021.

Han, S. W. and Kim, K.: Infrared matrix isolation study of acetone and methanol in solid argon, *J. Phys. Chem.*, 100, 17124-17132, 10.1021/jp961538n, 1996.

Harvey, R. M., Bateman, A. P., Jain, S., Li, Y. J., Martin, S., and Petrucci, G. A.: Optical Properties of Secondary Organic Aerosol from cis-3-Hexenol and cis-3-Hexenyl Acetate: Effect of Chemical Composition, Humidity, and Phase, *Environ. Sci. Technol.*, 50, 4997-5006, 10.1021/acs.est.6b00625, 2016.

Hassan, Z., Stahlberger, M., Rosenbaum, N., and Braese, S.: Criegee Intermediates Beyond Ozonolysis: Synthetic and

- Mechanistic Insights, *Angew. Chem. Int. Edit.*, **60**, 15138–15152, 10.1002/anie.202014974, 2021.
- Helmig, D., Daly, R. W., Milford, J., and Guenther, A.: Seasonal trends of biogenic terpene emissions, *Chemosphere*, **93**, 35-46, 10.1016/j.chemosphere.2013.04.058, 2013.
- Hofzumahaus, A., Rohrer, F., Lu, K. D., Bohn, B., Brauers, T., Chang, C. C., Fuchs, H., Holland, F., Kita, K., Kondo, Y., Li, X., Lou, S. R., Shao, M., Zeng, L. M., Wahner, A., and Zhang, Y. H.: Amplified Trace Gas Removal in the Troposphere, *Science*, **324**, 1702-1704, 10.1126/science.1164566, 2009.
- Jiang, H. T., Xie, C. L., Liu, Y., Xiao, C. L., Zhang, W. Q., Li, H. W., Long, B., Dong, W. R., Truhlar, D. G., and Yang, X. M.: Criegee Intermediates Significantly Reduce Atmospheric $(\text{CF}_3)_2\text{CFCN}$, *J. Am. Chem. Soc.*, **147**, 12263-12272, 10.1021/jacs.5c01737, 2025.
- Jokinen, T., Sipila, M., Richters, S., Kerminen, V. M., Paasonen, P., Stratmann, F., Worsnop, D., Kulmala, M., Ehn, M., Herrmann, H., and Berndt, T.: Rapid Autoxidation Forms Highly Oxidized RO_2 Radicals in the Atmosphere, *Angew. Chem. Int. Edit.*, **53**, 14596-14600, 10.1002/anie.201408566, 2014.
- Jr-Min Lin, J. and Chao, W.: Structure-dependent reactivity of Criegee intermediates studied with spectroscopic methods, *Chem. Soc. Rev.*, **46**, 7483-7497, 10.1039/C7CS00336F, 2017.
- Khan, M. A. H., Percival, C. J., Caravan, R. L., Taatjes, C. A., and Shallcross, D. E.: Criegee intermediates and their impacts on the troposphere, *Environ. Sci.-Proc. Imp.*, **20**, 437-453, 10.1039/c7em00585g, 2018.
- Kidwell, N. M., Li, H., Wang, X., Bowman, J. M., and Lester, M. I.: Unimolecular dissociation dynamics of vibrationally activated CH_3CHOO Criegee intermediates to OH radical products, *Nature Chemistry*, **8**, 509-514, 10.1038/nchem.2488, 2016.
- Kostiainen, R.: Volatile organic compounds in the indoor air of normal and sick houses, *Atmos. Environ.*, **29**, 693-702, 10.1016/1352-2310(94)00309-9, 1995.
- Lelieveld, J., Gromov, S., Pozzer, A., and Taraborrelli, D.: Global tropospheric hydroxyl distribution, budget and reactivity, *Atmos. Chem. Phys.*, **16**, 12477-12493, 10.5194/acp-16-12477-2016, 2016.
- Lin, H.-Y., Huang, Y.-H., Wang, X., Bowman, J. M., Nishimura, Y., Witek, H. A., and Lee, Y.-P.: Infrared identification of the Criegee intermediates syn- and anti- CH_3CHOO , and their distinct conformation-dependent reactivity, *Nat. Commun.*, **6**, 7012, 10.1038/ncomms8012, 2015.
- Lin, L. C., Chang, H. T., Chang, C. H., Chao, W., Smith, M. C., Chang, C. H., Lin, J. J. M., and Takahashi, K.: Competition between H_2O and $(\text{H}_2\text{O})_2$ reactions with $\text{CH}_2\text{OO}/\text{CH}_3\text{CHOO}$, *Phys. Chem. Chem. Phys.*, **18**, 4557-4568, 10.1039/c5cp06446e, 2016.
- Lin, Y.-H., Yin, C., Lin, W.-H., Li, Y.-L., Takahashi, K., and Lin, J. J.-M.: Criegee Intermediate Reaction with Alcohol Is Enhanced by a Single Water Molecule, *J. Phys. Chem. Lett.*, **9**, 7040-7044, 10.1021/acs.jpcclett.8b03349, 2018.
- Liu, D., Zhang, Y., Zhong, S., Chen, S., Xie, Q., Zhang, D., Zhang, Q., Hu, W., Deng, J., Wu, L., Ma, C., Tong, H., and Fu, P.: Large differences of highly oxygenated organic molecules (HOMs) and low-volatile species in secondary organic aerosols

- 550 (SOAs) formed from ozonolysis of β -pinene and limonene, *Atmos. Chem. Phys.*, 23, 8383-8402, 10.5194/acp-23-8383-2023, 2023.
- [Liu, S., Galeazzo, T., Valorso, R., Shiraiwa, M., Faiola, C. L., and Nizkorodov, S. A.: Secondary Organic Aerosol from OH-Initiated Oxidation of Mixtures of d-Limonene and beta-Myrcene, *Environ. Sci. Technol.*, 10.1021/acs.est.4c04870, 2024.](#)
- Long, B., Bao, J. L., and Truhlar, D. G.: Unimolecular reaction of acetone oxide and its reaction with water in the atmosphere, *Proc. Natl. Acad. Sci. U. S. A.*, 115, 6135-6140, 10.1073/pnas.1804453115, 2018.
- [Long, B., Bao, J. L., and Truhlar, D. G.: Rapid unimolecular reaction of stabilized Criegee intermediates and implications for atmospheric chemistry, *Nat. Commun.*, 10, 2003, 10.1038/s41467-019-09948-7, 2019.](#)
- Long, B., Xie, C., and Truhlar, D. G.: Criegee Intermediates Compete Well with OH as a Cleaning Agent for Atmospheric Amides, *J. Am. Chem. Soc.*, 10.1021/jacs.5c07439, 2025.
- 560 Lu, T.: Molclus, Version 1.1.2., <http://www.keinsci.com/research/molclus.html> (November 6, 2024), 2023.
- Luo, Y., Franzon, L., Zhang, J., Sarnela, N., Donahue, N. M., Kurten, T., and Ehn, M.: Gas-phase observations of accretion products from stabilized Criegee intermediates in terpene ozonolysis with two dicarboxylic acids, *Atmos. Chem. Phys.*, 25, 4655-4664, 10.5194/acp-25-4655-2025, 2025.
- Mauldin, R. L., Berndt, T., Sipilä, M., Paasonen, P., Petäjä, T., Kim, S., Kurtén, T., Stratmann, F., Kerminen, V. M., and Kulmala, M.: A new atmospherically relevant oxidant of sulphur dioxide, *Nature*, 488, 193-196, 10.1038/nature11278, 2012.
- 565 Munshi, H. B., Rao, K., and Iyer, R. M.: Rate constants of the reactions of ozone with nitriles, acrylates and terpenes in gas-phase, *Atmos. Environ.*, 23, 1971-1976, 10.1016/0004-6981(89)90522-2, 1989.
- Neese, F.: Software update: The ORCA program system-Version 5.0, *WIREs Comput. Mol. Sci.*, 10.1002/wcms.1606, 2022.
- Newland, M. J., Rickard, A. R., Sherwen, T., Evans, M. J., Vereecken, L., Munoz, A., Rodenas, M., and Bloss, W. J.: The atmospheric impacts of monoterpene ozonolysis on global stabilised Criegee intermediate budgets and SO₂ oxidation: experiment, theory and modelling, *Atmos. Chem. Phys.*, 18, 6095-6120, 10.5194/acp-18-6095-2018, 2018.
- [Peräkylä, O., Berndt, T., Franzon, L., Hasan, G., Meder, M., Valiev, R. R., Daub, C. D., Varelas, J. G., Geiger, F. M., Thomson, R. J., Rissanen, M., Kurtén, T., and Ehn, M.: Large Gas-Phase Source of Esters and Other Accretion Products in the Atmosphere, *J. Am. Chem. Soc.*, 145, 7780-7790, 10.1021/jacs.2c10398, 2023.](#)
- 575 Ringsdorf, A., Edtbauer, A., Vila-Guerau de Arellano, J., Pfannerstill, E. Y., Gromov, S., Kumar, V., Pozzer, A., Wolff, S., Tsokankunku, A., Soergel, M., Sa, M. O., Araujo, A., Ditas, F., Poehlker, C., Lelieveld, J., and Williams, J.: Inferring the diurnal variability of OH radical concentrations over the Amazon from BVOC measurements, *Sci. Rep.*, 13, 10.1038/s41598-023-41748-4, 2023.
- Sindelarova, K., Granier, C., Bouarar, I., Guenther, A., Tilmes, S., Stavrou, T., Muller, J. F., Kuhn, U., Stefani, P., and Knorr, W.: Global data set of biogenic VOC emissions calculated by the MEGAN model over the last 30 years, *Atmos. Chem. Phys.*, 14, 9317-9341, 10.5194/acp-14-9317-2014, 2014.
- 580

- Sipila, M., Jokinen, T., Berndt, T., Richters, S., Makkonen, R., Donahue, N. M., Mauldin, R. L., III, Kurten, T., Paasonen, P., Sarnela, N., Ehn, M., Junninen, H., Rissanen, M. P., Thornton, J., Stratmann, F., Herrmann, H., Worsnop, D. R., Kulmala, M., Kerminen, V. M., and Petaja, T.: Reactivity of stabilized Criegee intermediates (sCIs) from isoprene and monoterpene ozonolysis toward SO₂ and organic acids, *Atmos. Chem. Phys.*, 14, 12143-12153, 10.5194/acp-14-12143-2014, 2014.
- 585 Su, Y.-T., Huang, Y.-H., Witek, H. A., and Lee, Y.-P.: Infrared Absorption Spectrum of the Simplest Criegee Intermediate CH₂OO, *Science*, 340, 174-176, 10.1126/science.1234369, 2013.
- Su, Y.-T., Lin, H.-Y., Putikam, R., Matsui, H., Lin, M. C., and Lee, Y.-P.: Extremely rapid self-reaction of the simplest Criegee intermediate CH₂OO and its implications in atmospheric chemistry, *Nat. Chem.*, 6, 477-483, 10.1038/nchem.1890, 2014.
- 590 Taatjes, C. A., Welz, O., Eskola, A. J., Savee, J. D., Scheer, A. M., Shallcross, D. E., Rotavera, B., Lee, E. P. F., Dyke, J. M., Mok, D. K. W., Osborn, D. L., Percival, C. J. : Direct Measurements of Conformer-Dependent Reactivity of the Criegee Intermediate CH₃CHOO, *Science*, 340, 177-180, 10.1126/science.1234689, 2013.
- Vereecken, L., Harder, H., and Novelli, A.: The reaction of Criegee intermediates with NO, RO₂, and SO₂, and their fate in the atmosphere, *Phys. Chem. Chem. Phys.*, 14, 14682-14695, 10.1039/c2cp42300f, 2012.
- 595 Vereecken, L., Novelli, A., and Taraborrelli, D.: Unimolecular decay strongly limits the atmospheric impact of Criegee intermediates, *Phys. Chem. Chem. Phys.*, 19, 31599-31612, 10.1039/c7cp05541b, 2017.
- Vereecken, L., Novelli, A., Kiendler-Scharr, A., and Wahner, A.: Unimolecular and water reactions of oxygenated and unsaturated Criegee intermediates under atmospheric conditions, *Phys. Chem. Chem. Phys.*, 24, 6428-6443, 10.1039/d1cp05877k, 2022.
- 600 Wang, Y.-Y., Chung, C.-Y., and Lee, Y.-P.: Infrared spectral identification of the Criegee intermediate (CH₃)₂COO, *J. Chem. Phys.*, 145, 154303, 10.1063/1.4964658, 2016.
- Wang, Z., Tong, S. R., Chen M. F., Jing, B., Li, W. R., Guo, Y. C., Ge, M. F., Wang, S. F.: Study on ozonolysis of asymmetric alkenes with matrix isolation and FT-IR spectroscopy, *Chemosphere*, 252, 126413, 10.1016/j.chemosphere.2020.126413, 2020.
- 605 Welz, O., E. A. J., Sheps L., Rotavera B., Savee J. D., Scheer A. M., Osborn D. L., Lowe D., Booth A. M., Xiao P., Khan M. A. H., Percival C. J., Shallcross D. E.: Rate Coefficients of C1 and C2 Criegee Intermediate Reactions with Formic and Acetic Acid Near the Collision Limit: Direct Kinetics Measurements and Atmospheric Implications, *Angew. Chem. Int. Edit.*, 53, 4547-4550, 10.1002/anie.201400964, 2014.
- Yang, X., Deng, J., Li, D., Chen, J., Xu, Y., Zhang, K., Shang, X., and Cao, Q.: Transient species in the ozonolysis of tetramethylethene, *J. Environ. Sci.*, 95, 210-216, 10.1016/j.jes.2020.03.027, 2020.
- 610 Yin, C. and Takahashi, K.: Effect of unsaturated substituents in the reaction of Criegee intermediates with water vapor, *Phys. Chem. Chem. Phys.*, 20, 20217-20227, 10.1039/c8cp02064g, 2018.
- Yu, S. S., Tong, S. R., Chen, M. F., Zhang, H. L., Xu, Y. Y., Guo, Y. C., and Ge, M. F.: Characterization of Key Intermediates and Products from the Ozonolysis of Styrene-Like Compounds, *Environ. Sci. Technol.*, 10.1021/acs.est.5c00769, 2025.

- 615 Zhang, D. and Zhang, R.: Ozonolysis of alpha-pinene and beta-pinene: Kinetics and mechanism, *J. Chem. Phys.*, 122, 10.1063/1.1862616, 2005.
- Zhang, S., Du, L., Yang, Z., Tchinda, N. T., Li, J., and Li, K.: Contrasting impacts of humidity on the ozonolysis of monoterpenes: insights into the multi-generation chemical mechanism, *Atmos. Chem. Phys.*, 23, 10809-10822, 10.5194/acp-23-10809-2023, 2023.
- [Zhao, Q., Wang, W., Liu, F., Lu, J., and Wang, W.: Oligomerization reactions for precursors to secondary organic aerosol: Comparison between two formation mechanisms for the oligomeric hydroxyalkyl hydroperoxides, *Atmos. Environ.*, 166, 1-8, 10.1016/j.atmosenv.2017.07.008, 2017.](#)
- 620 Zhao, Y., Wingen, L. M., Perraud, V., Greaves, J., and Finlayson-Pitts, B. J.: Role of the reaction of stabilized Criegee intermediates with peroxy radicals in particle formation and growth in air, *Phys. Chem. Chem. Phys.*, 17, 12500-12514, 10.1039/c5cp01171j, 2015.
- 625 Zhao, Z., Zhang, W., Alexander, T., Zhang, X., Martin, D. B. C., and Zhang, H.: Isolating α -Pinene Ozonolysis Pathways Reveals New Insights into Peroxy Radical Chemistry and Secondary Organic Aerosol Formation, *Environ. Sci. Technol.*, 55, 6700-6709, 10.1021/acs.est.1c02107, 2021.